JOC The Journal of Organic Chemistry

Article

pubs.acs.org/joc

Charge-Transfer Emission in Organoboron-Based Biphenyls: Effect of Substitution Position and Conformation

Chen Wang,[†] Qing-Wen Xu,[†] Wei-Ning Zhang,[†] Qian Peng,[‡] and Cui-Hua Zhao*[,†]

[†]School of Chemistry and Chemical Engineering, Key Laboratory of Special Functional Aggregated Materials, Ministry of Education, Shandong University, Jinan 250100, People's Republic of China

[‡]Beijing National Laboratory for Molecular Sciences, Key Laboratory of Organic Solids, Institute of Chemistry, Chinese Academy of Sciences, Beijing 100190, People's Republic of China

Supporting Information

ABSTRACT: A series of organoboron-based biphenyls ***o,o′*-NMe$_2$**, ***o,p′*-NMe$_2$**, ***p,p′*-NMe$_2$**, which contain an electron-donating NMe_2 and an electron-accepting $BMes_2$ groups at *o,o′*-, *o,p′*-, *p,p′*-positions of biphenyl skeleton, respectively, as well as ***o,o′*-NBn$_2$**, which contains more bulky NBn_2 rather than NMe_2, were fully characterized to explore the effect of structural modification on the intramolecular charge-transfer emissions. In addition to significant effect of substitution position on photophysical properties, remarkable influence of conformation was also observed for *o,o′*-substituted compounds. The emission is substantially blue-shifted as conformation changes from the location of NMe_2 and $BMes_2$ at same side of biphenyl axis with a close B···N distance, and thus direct B···N electronic interaction in ***o,o′*-NMe$_2$**, to the location of NBn_2 and $BMes_2$ on two opposite sides in ***o,o′*-NBn$_2$**. And ***o,o′*-NMe$_2$** exhibits the longest emission wavelength, but the shortest absorption wavelength, and thus largest Stokes shift among these four organoboron-based biphenyls in both solution and solid state. The theoretical calculations demonstrated that the unique structure of ***o,o′*-NMe$_2$**, in which boryl and amino located at the same side of biphenyl axis with close B···N distance and direct B···N electronic interaction, is helpful to stabilize the lowest singly occupied orbital in the exited state.

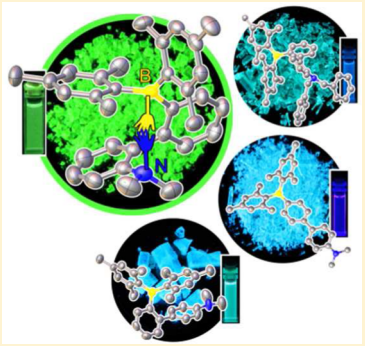

INTRODUCTION

Organic fluorophores have been widely applied in a broad range of fields, such as, chemical sensors, biomolecular labels, cellular stains for chemical biology research, medical diagnosis, and organic light-emitting diodes.[1] The photophysical properties of organic fluorophores are mainly characterized by UV−vis absorption and fluorescence spectra, molar extinction coefficient, quantum yield, and Stokes shift. Among these photophysical properties, a large Stokes shift is greatly preferred as the large Stokes shift not only helps to minimize the self-quenching effect but also boosts the signal-to-noise ratio in bioimaging applications owing to the great separation between excitation and emission wavelengths.[2] In addition, a high fluorescence quantum efficiency especially in the solid state is highly desirable due to high relevance of quantum yield to fluorescence brightness and versatile utility of fluorophores in the solid-state form.[3] However, most fluorophores show very weak fluorescence or even no fluorescence in the solid state due to the severe aggregation-caused quenching effect as the result of certain intermolecular interactions, such as aggregate or excimer formation and energy migration in the solid state.[3b,4] Although several effective approaches have been developed to achieve solid-state emissive fluorophores, such as bulky or dendritic substituent protection,[5] cross-dipole stacking,[6] taking advantage of aggregation-induced emission,[7−9] *J*-aggregation formation,[10] the spiro concept,[11] and enhanced intramolecular charge-transfer emission,[12−14] it still remains a very challenging issue to obtain solid-state fluorescence with particularly large Stokes shift.

To obtain fluorescent materials, the triarylboron-based molecules have recently attracted remarkable interest. One notable feature of boron in conjugated three-coordinate organoborons is its strong electron-accepting ability through p_π−π^* conjugation between vacant p orbital of boron with π^* of π-conjugated framework.[15] When an electron-donating group is present, the triarylboron-systems usually display strong intramolecular charge-transfer (CT) characteristics, which make them promising materials for applications in nonlinear optics,[16,17] organic light-emitting diodes (OLEDs),[18−20] and ion sensing.[21−24] In addition, it is effective to achieve solid-state emission via introduction of bulky electron-accepting dimesitylboryl ($BMes_2$) group at the side position of electron-donating π-conjugated framework. The success of this molecular design is ascribed to two kinds of effect of lateral boryl groups.[12] One is the steric bulkiness, which can suppress the intermolecular interaction. The other is the electron-accepting ability, which can induce a large Stokes shift as the result of intramolecular CT transition and thus efficiently prevent fluorescence self-quenching in the condensed state. As a result, the lateral boryl-substituted π-system is capable of fulfilling both high solid-state fluorescence efficiency and large

Received: September 1, 2015
Published: October 1, 2015

DOI: 10.1021/acs.joc.5b02038
J. Org. Chem. 2015, 80, 10914−10924

Stokes shift. The largest Stokes shift is up to 195 nm in polar THF solvent and 178 nm in the spin-coated film.[12b] Based on the design concept of lateral boryl-substituted π-system, we have recently disclosed another solid-state emissive organoboron π-system, in which the bulky electron-accepting $BMes_2$ and electron-donating dimethylamino (NMe_2) groups are introduced at the o,o'- positions of biphenyl framework (***o,o'*-NMe$_2$**, Figure 1).[25] In addition to high solid-state fluorescence

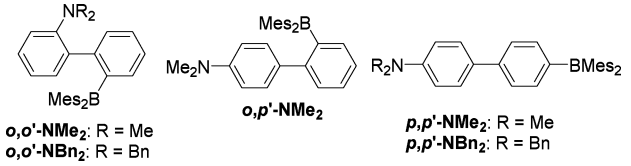

Figure 1. Molecular structure of organoboron-based biphenyls.

efficiency (Φ_F = 0.86 for the spin-coated film), another notable feature for this organoboron-based biphenyl is that the Stokes shift is particularly large, more than 200 nm ($\Delta\lambda$ = 215 nm in cyclohexane and spin-coated film; 277 nm in acetonitrile), which is unusual for the normal CT emitting organoborons. Compared with its regioisomers, ***p,p'*-NMe$_2$** and ***o,p'*-NMe$_2$**, in which $BMes_2$ and NMe_2 groups are introduced at different positions, ***o,o'*-NMe$_2$** displays much shorter absorption but much longer emission in both solution and spin-coated film.[25a,b] Moreover, it was newly found that the simple displacement of NMe_2 by NBn_2 (***o,o'*-NBn$_2$**) can lead to remarkable blue shift in emission ($\Delta\lambda$ = 71 nm in cyclohexane; 62 nm in spin-coated film), while the change of absorption is trivial. However, the electron-donating abilities of NBn_2 and NMe_2 are very close. And thus it is the steric effect difference that is expected to account for such a great hypsochromism of emission. Inspired by the fascinating properties of ***o,o'*-NMe$_2$** and the significant influence of substitution pattern and steric effect of amino group on photophysical properties, we are interested in the underlying reasons. The elucidation of these points will provide a very useful basis for the further design of fascinating organoborons, especially those with high solid-state fluorescence efficiency and large Stokes shift. Herein, we have fully investigated the single-crystal X-ray structures, UV−vis absorption, steady-state fluorescence, time-resolved fluorescence, and theoretically calculated structures in ground state and excited state for a series of triarylboron-based biphenyls, including ***o,o'*-NMe$_2$**, ***o,p'*-NMe$_2$**, ***p,p'*-NMe$_2$**, and ***o,o'*-NBn$_2$**, in which the boryl and amino groups are introduced at different positions or the substituents of amino group are varied for o,o'-substituted compounds(Figure 1). Here, ***p,p'*-NBn$_2$** was also designed to prove that NBn_2 has an electron-donating ability similar to that of NMe_2 through comparison of its photophysical properties with those of ***p,p'*-NMe$_2$**.

RESULTS AND DISCUSSION

Synthesis. The regioisomeric biphenyls ***o,o'*-NMe$_2$**, ***o,p'*-NMe$_2$**, and ***p,p'*-NMe$_2$** were prepared in our previous work.[25a] The synthetic routes to other remaining molecules ***o,o'*-NBn$_2$** and ***p,p'*-NBn$_2$** are shown in Scheme 1. They were both facilely synthesized from their corresponding brominated precursors **1** and **2**. The lithiation of brominated biphenyls of **1** and **2** with *n*-BuLi at −78 °C followed by treatment with dimesitylfluoroborane afforded the corresponding borylated compounds in moderate yields. The preparation of brominated precursor **1** for

Scheme 1. Synthesis of Organoboron-Based Biphenyls[a]

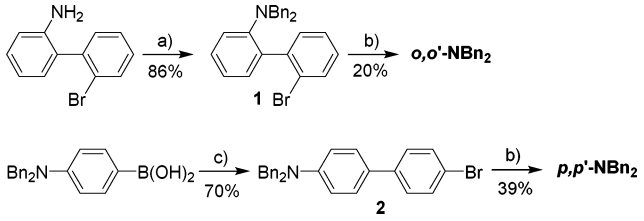

[a]Reagents and conditions: (a) BnBr, K_2CO_3, CH_3CN, 90 °C; (b) (i) *n*-BuLi, THF, − 78 °C, 1h; (ii) Mes_2BF, THF, − 78 °C to RT; (c) 4-iodobromobenzene, K_2CO_3, $Pd(OAc)_2$, PPh_3, toluene, H_2O/EtOH (3/1), reflux.

***o,o'*-NBn$_2$**, was easily achieved via benzylation of the corresponding amino starting materials, 2-amino-2′-bromobiphenyl. And the brominated precursor **2** for ***p,p'*-NBn$_2$** was obtained through Pd-catalyzed Suzuki cross-coupling reaction of [(4-dibenzylamino)phenyl] boronic acid with 4-iodobromobenzene. Similar to other organoboron-based biphenyls, ***o,o'*-NBn$_2$** and ***p,p'*-NBn$_2$** are also very stable in air and water and can be purified by silica-gel column chromatography. They were fully characterized by ^1H and ^{13}C NMR spectroscopy and high-resolution mass spectrometry.

Crystal Structures. The newly prepared organoboron-based biphenyl ***o,o'*-NBn$_2$** was characterized by X-ray crystallography. The single crystals suitable for X-ray diffraction were obtained by slow evaporation of the corresponding solution in a mixed CH_2Cl_2/MeOH solvent. For a comprehensive comparison, the X-ray crystal structures of the regioisomeric biphenyls, ***o,o'*-NMe$_2$**,[25a] ***o,p'*-NMe$_2$**,[25b] and ***p,p'*-NMe$_2$**[17c] were also analyzed in great details. The X-ray crystal structures are shown in Figure 2, and selected bond lengths and dihedral angle are listed in Table 1. For convenience, the amino-bonded phenyl ring is labeled as P1. Another phenyl ring of biphenyl framework and two phenyl rings of mesityl groups are labeled as P2, P3, and P4, respectively.

With regard to the X-ray structures of these organoboron-based biphenyls, the following three findings are noted. (1)

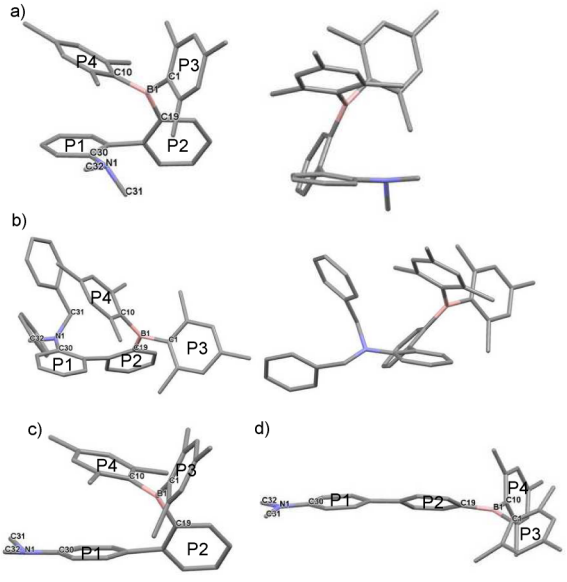

Figure 2. Crystal structures of (a) ***o,o'*-NMe$_2$**; (b) ***o,o'*-NBn$_2$**; (c) ***o,p'*-NMe$_2$**; and (d) ***p,p'*-NMe$_2$**. Hydrogen atoms are omitted for clarity.

DOI: 10.1021/acs.joc.5b02038
J. Org. Chem. 2015, 80, 10914−10924

Table 1. Selected Bond Lengths (Å), Distances (Å), Bond Angles (°), and Dihedral Angles (°) for Organoboron-Based Biphenyls

	o,o′-NMe_2	*o,o′*-NBn_2	*o,p′*-NMe_2	*p,p′*-NMe_2
B1−C1	1.590	1.572	1.585	1.574
B1−C10	1.578	1.577	1.559	1.576
B1−C19	1.579	1.580	1.580	1.561
N1−C30	1.425	1.408	1.402	1.378
∑∠C−B−C	359.8	359.7	359.7	360.0
∑∠C−N−C	340.4	352.7	355.1	359.6
∠P2−BC_3	30.3	36.7	39.0	30.9
∠P3−BC_3	55.4	54.8	63.8	66.7
∠P4−BC_3	53.8	58.5	52.8	42.9
∠P1−P2	70.7	50.0	56.4	25.8
∠P1−P4	27.3	37.5	18.8	—
centroid−centroid distance (P1−P4)	3.87	4.07	3.64	—
B···N distance	3.59	4.76	6.28	10.09

Most interestingly, the relative positions of amino and boryl groups are completely different for ***o,o′*-NMe$_2$** and ***o,o′*-NBn$_2$**. In ***o,o′*-NMe$_2$**, the biphenyl skeleton is highly twisted with a torsion angle of 70.7°. Despite the great steric congestion between boryl and amino groups, they are still arranged at the same side of biphenyl axis with a close B···N distance (3.59 Å). The very close B···N distance might suggest possible direct electronic attraction between boryl and amino groups.[25a] In contrast, ***o,o′*-NBn$_2$** adopts a conformation, in which boryl and amino groups are located on two opposite sides of biphenyl axis. This change in the relative positions of boryl and amino groups is probably due to the significant steric bulk of NBn_2, which would make the electronic B···N interaction become impossible. The location of boryl and amino groups on two opposite sides of biphenyl axis is expected to be helpful to minimize steric repulsion between them. Meanwhile, biphenyl framework turns more coplanar from ***o,o′*-NMe$_2$** to ***o,o′*-NBn$_2$** (dihedral angle between P1 and P2: 70.7° for ***o,o′*-NMe$_2$**; 50.0° for ***o,o′*-NBn$_2$**). The torsion angle between P1 and P2 in ***o,o′*-NBn$_2$** is even slightly smaller than ***o,p′*-NMe$_2$**, although ***o,o′*-NBn$_2$** contains one more bulky NBn_2 substituent at lateral position (dihedral angle between P1 and P2 for ***o,p′*-NMe$_2$**: 56.4°). The increased coplanarity of biphenyl unit in ***o,o′*-NBn$_2$** is also supposed to be beneficial to release steric repulsion between boryl and amino groups since the smaller the dihedral angle between P1 and P2, the longer distance between boryl and amino groups. With regard to ***p,p′*-NMe$_2$**, it is easily understandable that the biphenyl unit is much more coplanar than the other two regioisomers due to absence of bulky lateral substituents. (2) In addition, it was noted that the geometries of nitrogen center are quite different, although boron center has very similar structure. The boron-centered BC_3 moieties are all perfectly planar irrespective of their positions, with the sum of C−B−C bond angles equal to 360°. The BC_3 planes and phenyl rings (P3 and P4) of two mesityl groups form dihedral angles within the range of 42.9−66.7°, while the phenyl ring (P2) of biphenyl skeleton is twisted out of BC_3 planes by much lower dihedral angles (30.3−39.0°). It seems the coplanarity between BC_3 plane and B-bonded phenyl ring has little influence on B−C bond lengths. The B−C bond lengths (1.572−1.590 Å) are very close with exception of slightly shorter bond length of B−C19 (1.561 Å) in ***p,p′*-NMe$_2$** and B−C10 (1.559 Å) in ***o,p′*-NMe$_2$**, suggesting possible more efficient electron delocalization between B center and corresponding phenyl rings. In contrast to the similar structure of the boron center, the geometry of nitrogen center varies with its substitution position and the substituent on it. In ***p,p′*-NMe$_2$**, the NC_3 plane shows a completely planar structure, in which the sum of C−N−C bond angle is 360°. From ***p,p′*-NMe$_2$** to ***o,p′*-NMe$_2$** and ***o,o′*-NMe$_2$**, the NC_3 plane turns incrementally pyramidalized (sum of C−N−C bond angles: 355.1° for ***o,p′*-NMe$_2$**; 340.4° for ***o,o′*-NMe$_2$**). Moreover, the planarity of NC_3 plane exhibits great effect on N−C30 bond length and thus conjugation between N center and its bonded P1 ring. With the increased pyramidalization of NC_3 plane, N−C30 bond length is elongated gradually (1.378 Å for ***p,p′*-NMe$_2$**; 1.402 Å for ***o,p′*-NMe$_2$**; 1.425 Å ***o,o′*-NMe$_2$**), denoting increasingly poorer electron delocalization of amino to the attached P1 ring. Notably, from ***o,o′*-NMe$_2$** to ***o,o′*-NBn$_2$**, as the result of released steric congestion between boryl and amino groups, the NC_3 plane becomes more planar with a shorter N−C30 bond length (sum of C−N−C bond angles: 352.7°; N−C30 bond length 1.408 Å for ***o,o′*-NBn$_2$**) and thus more efficient conjugation between amino and P1. (3) Another notable thing is the possible intramolecular $\pi-\pi$ interaction between P1 and P4 when the boryl group is located at the lateral *o*-position, as evidenced by small torsion angle (18.8−37.5°) and centroid−centroid distance (3.64−4.07 Å) between P1 and P4. Comparatively, this $\pi-\pi$ interaction of ***o,o′*-NBn$_2$** should be much weaker than that of ***o,o′*-NMe$_2$** and ***o,p′*-NMe$_2$**, judging from larger torsion angle and longer centroid−centroid distance between P1 and P4 in ***o,o′*-NBn$_2$**. The above detailed analyses on the X-ray structures clearly demonstrate that both substitution position of boryl and amino groups and steric effect of amino exhibit remarkable influence on molecular structures, which would supposedly affect electronic structures and thus photophysical properties.

Photophysical Properties in Cyclohexane. All these biphenyls contain both electron-withdrawing boryl and electron-donating amino groups, and they are expected to show typical intramolecular CT emission. To eliminate the solvent effect on fluorescence, their photophysical properties were first measured in nonpolar cyclohexane. The UV−vis absorption and emission spectra are shown in Figure 3, and the corresponding data are summarized in Table 2.

Among the three regioisomeric biphenyls, in which NMe_2 and $BMes_2$ are introduced at different positions, ***o,o′*-NMe$_2$** shows the shortest absorption and the longest emission wavelengths and thus the largest Stokes shift. The Stokes shift of ***o,o′*-NMe$_2$** is more than 200 nm, which is very rare for

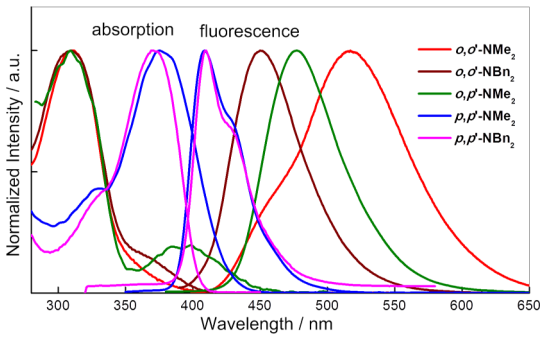

Figure 3. Absorption and fluorescence spectra of organoboron-based biphenyls.

DOI: 10.1021/acs.joc.5b02038
J. Org. Chem. 2015, 80, 10914−10924

Table 2. UV−vis Absorption and Fluorescence Data for Biphenyls Containing Boryl and Amino Groups in Nondegassed Cyclohexane

	absorption		emission		Stokes shift		excited dynamics		
	λ_{abs} (nm)[a]	log ε	λ_{em} (nm)	Φ_F[b]	$\Delta\nu$ (cm^{-1})	$\Delta\lambda$	τ (ns)	k_r (s^{-1})	k_{nr} (s^{-1})
***o,o′*-NMe$_2$**	306	4.74	521	0.47	13485	215	17.8	2.64×10^7	2.98×10^7
***o,o′*-NBn$_2$**	362[c]	3.45	450	0.43	5402	88	9.81	4.38×10^7	5.81×10^7
***o,p′*-NMe$_2$**	388	3.48	477	0.72	4808	89	11.6	6.20×10^7	2.41×10^7
***p,p′*-NMe$_2$**	369	4.50	409	0.95	2650	40	1.64	5.79×10^8	3.05×10^7
***p,p′*-NBn$_2$**	371	4.61	410	0.68	2564	39	—	—	—

[a]Only the longest absorption maximum wavelengths are given. [b]Calculated by using fluorescein as a standard.[26] [c]Observed as a shoulder.

the general intramolecular CT emitting system. The very short absorption wavelength of ***o,o′*-NMe$_2$** is easily explainable (λ_{abs} = 306 nm). One possible reason is that the absorption band corresponding to the first excited-state (S_1) transition, which essentially consists of an intramolecular CT transition from HOMO located on amino phenyl moiety to LUMO localized on boryl phenyl unit, is too weak to be distinguished due to the poor overlap between HOMO and LUMO as the result of the significantly twisted structure of biphenyl skeleton. On the contrary, ***o,p′*-NMe$_2$** and ***p,p′*-NMe$_2$** show distinct intramolecular CT absorption bands with ***o,p′*-NMe$_2$** displaying longest absorption wavelength (λ_{abs} = 388 nm for ***o,p′*-NMe$_2$**; 369 nm for ***p,p′*-NMe$_2$**) and ***p,p′*-NMe$_2$** having the highest absorptivity (log ε = 3.48 for ***o,p′*-NMe$_2$**; 4.50 for ***p,p′*-NMe$_2$**).[25a,b] It is totally out of expectation that the emission of ***o,o′*-NMe$_2$** is much longer than both ***o,p′*-NMe$_2$** and ***p,p′*-NMe$_2$** (λ_{em} = 521 nm for ***o,p′*-NMe$_2$**; 477 nm for ***o,p′*-NMe$_2$**; 409 nm for ***o,p′*-NMe$_2$**) considering more pyramidalized geometry of amino center and more twisted structure of biphenyl skeleton, which would theoretically lead to less efficient electron delocalization and thus lowered HOMO energy level. The very long emission wavelength of ***o,o′*-NMe$_2$** is another important reason for its particularly large Stokes shift. With regard to the fluorescence efficiency, the fluorescence quantum yield decreases gradually from ***p,p′*-NMe$_2$** to ***o,p′*-NMe$_2$** and ***o,o′*-NMe$_2$** (Φ_F = 0.47 for ***o,o′*-NMe$_2$**; 0.72 for ***o,p′*-NMe$_2$**; 0.95 for ***p,p′*-NMe$_2$**), which is in accordance with the change trend in absorptivity of lowest CT transition.[25a,b] Intriguingly, ***o,o′*-NMe$_2$** still retains very high quantum yield despite that the S_1-state transition is almost prohibited.

In the absorption spectra of ***o,o′*-NBn$_2$**, a weak shoulder band at 362 nm (log ε = 3.45) is observed in addition to the intense absorption band at 309 nm, which is completely overlapped with that of ***o,o′*-NMe$_2$**. The shoulder band at 362 nm is theoretically assigned to the intramolecular CT transition from HOMO to LUMO. The higher visibility of intramolecular CT band of ***o,o′*-NBn$_2$** relative to ***o,o′*-NMe$_2$** is probably ascribed to the following two possible reasons. One is a greater possibility of HOMO → LUMO transition due to greater coplanarity of biphenyl framework, which would lead to stronger overlap between HOMO and LUMO. Another is bathochromism in the HOMO → LUMO transition absorption band and thus larger separation from absorption of higher exited-state transition, because of higher planarity of N center and biphenyl skeleton, which would cause more efficient electron delocalization and therefore elevated HOMO energy level. Concomitant with bathochromism of absorption, the fluorescence was also supposed to shift to longer wavelength from ***o,o′*-NMe$_2$** to ***o,o′*-NBn$_2$**. In contrast, the emission is remarkably blue-shifted by 71 nm with quantum yield remaining almost unchanged. This prominent change of fluorescence should not arise from the difference of electron-donating ability between NMe_2 and NBn_2, but conformation difference of biphenyl skeleton due to greater steric effect of NBn_2 than NMe_2. To exclude the influence of electron-donating ability of amino group, the photophysical properties of ***p,p′*-NMe$_2$** were compared with those of ***p,p′*-NBn$_2$**. When amino group is located at terminal *p′*-position, its steric effect should has little influence on the structure of biphenyl framework. It was found that ***p,p′*-NBn$_2$** and ***p,p′*-NMe$_2$** have very similar absorption and fluorescence spectra, confirming close electron-donating ability of **NMe$_2$** and **NBn$_2$**. All these experimental results might imply that the special conformation of ***o,o′*-NMe$_2$**, in which amino and boryl groups are located at the same side of biphenyl axis with close contact and direct electronic interaction between boron and nitrogen centers, is essential for its long emission wavelength and particularly large Stokes shift.

To further elucidate the effect of structural modification on photophysical properties, we measured time-resolved fluorescence and determined the fluorescence lifetime (τ_s). In addition, the radiative (k_r) and nonradiative (k_{nr}) decay rate constants were also calculated. It was noted that ***o,o′*-NMe$_2$** shows a long fluorescence lifetime of 17.8 ns, which is much longer than those of ***o,p′*-NMe$_2$** and ***p,p′*-NMe$_2$** (τ = 11.6 ns for ***o,p′*-NMe$_2$**; 1.64 ns for ***p,p′*-NMe$_2$**). Judging from the calculated k_r and k_{nr}, it is the deceleration of radiative decay process that mainly accounts for the elongated fluorescence lifetime and decreased fluorescence quantum yield from ***p,p′*-NMe$_2$** to ***o,p′*-NMe$_2$** and ***o,o′*-NMe$_2$**. The deceleration of radiative process may arise from decreased efficiency of HOMO → LUMO transition due to increased noncoplanarity and thus weaker HOMO−LUMO overlap with more substituent in the lateral positions. Unexpectedly, the nonradiative decay rate constants are not very different for the three regioisomers, although the increasing noncoplanarity of biphenyl is supposed to promote nonradiative decay. The $\pi-\pi$ interaction between P1 and P4 in ***o,p′*-NMe$_2$** and ***o,o′*-NMe$_2$** and direct B···N electronic attraction in ***o,o′*-NMe$_2$** might play an important role for the suppression of the nonradiative decay. These interactions would make the molecular structure more rigid and thus restrict the free rotation of lateral substituents. It was also noted that from ***o,o′*-NMe$_2$** to ***o,o′*-NBn$_2$**, the radiative and nonradiative decays are accelerated with similar extent. This phenomenon can be explained in the following way. From ***o,o′*-NMe$_2$** to ***o,o′*-NBn$_2$**, with the change of relative position of boryl and amino groups from same side to opposite sides, the release of steric congestion of lateral groups leads to higher coplanarity of biphenyl and thus higher HOMO−LUMO overlap. As a consequence, the radiative decay is accelerated. Meanwhile, the lateral groups are expected to become more flexible with the release of steric congestion, which is presumably the possible reason for the acceleration of nonradiative decay.

DOI: 10.1021/acs.joc.5b02038
J. Org. Chem. 2015, 80, 10914−10924

Table 3. Selected Bond Lengths (Å), Distances (Å), Bond Angles (°), and Dihedral Angles (°) for Structures of the DFT-Optimized S_0 State and TD-DFT-Optimized S_1 State of Organoboron-Based Biphenyls[a]

	o,o′-NMe_2		*o,o′*-NBn_2		*o,p′*-NMe_2		*p,p′*-NMe_2	
	S_0	S_1	S_0	S_1	S_0	S_1	S_0	S_1
B1−C1	1.584	1.597	1.592	1.586	1.590	1.576	1.600	1.555
B1−C10	1.583	1.599	1.584	1.592	1.584	1.587	1.600	1.555
B1−C19	1.580	1.528	1.585	1.546	1.577	1.546	1.578	1.612
N1−C30	1.486	1.454	1.472	1.469	1.445	1.418	1.391	1.416
∑∠C−B−C	359.8	360.0	359.7	360.0	359.7	360.0	360.0	360.0
∑∠C−N−C	333.0	357.0	342.6	358.7	347.7	359.7	353.3	360.0
∠P2−BC3	37.4	17.0	38.9	26.9	36.9	24.3	24.8	48.2
∠P3−BC3	49.9	54.9	54.7	49.8	56.9	48.1	57.3	41.6
∠P4−BC3	53.7	56.7	51.2	55.0	48.3	52.5	57.3	41.6
∠P1−P2	70.7	65.5	40.5	47.3	44.3	63.6	41.0	27.3
∠P1−P4	25.8	22.7	51.5	38.8	39.7	23.7	—	—
centroid−centroid distance (P1−P4)	3.90	3.71	4.39	4.00	4.10	3.57	—	—

[a]Basis sets: 6-31G(d) for H, B, C; and 6-31G+(d) for N.

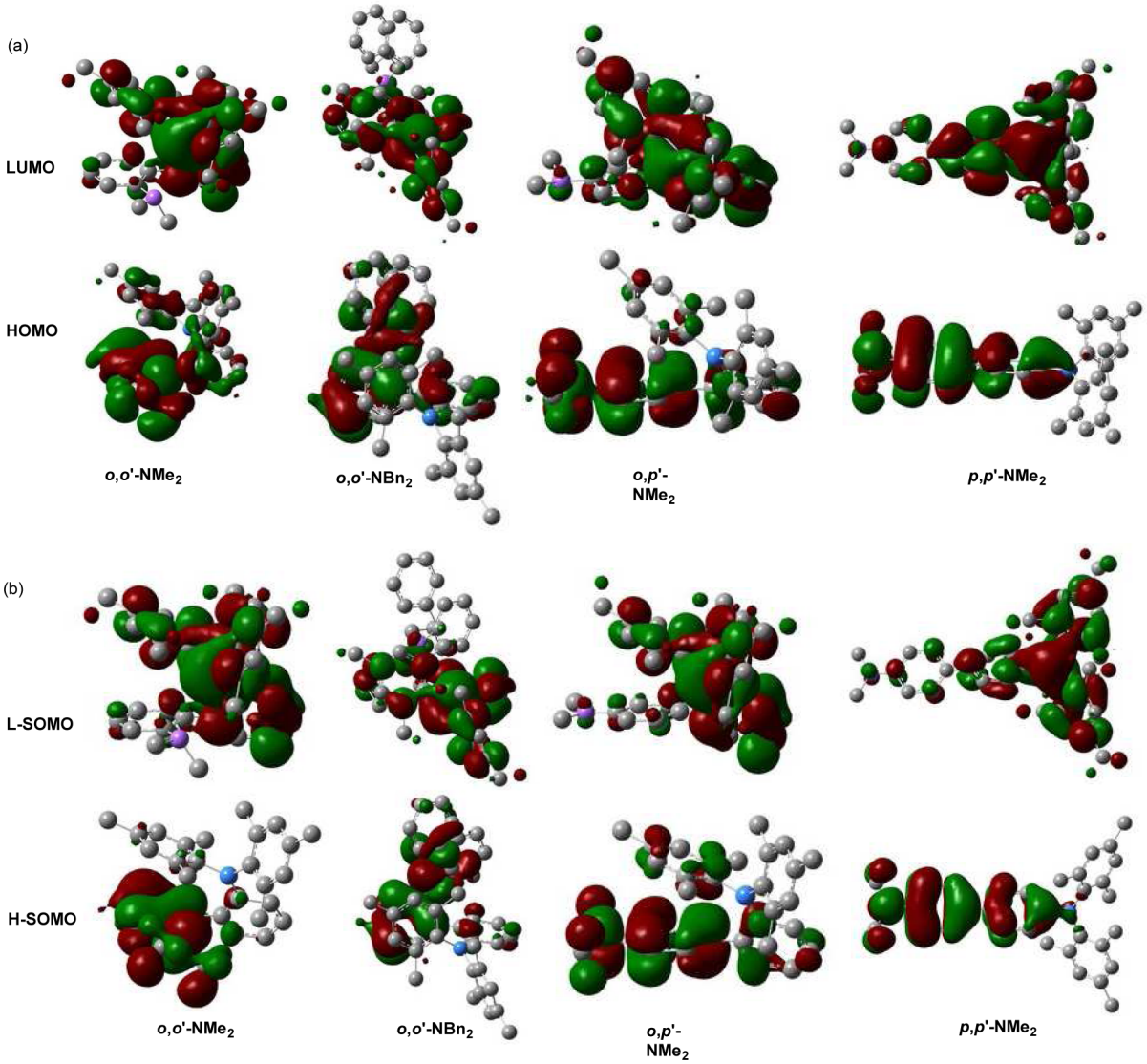

Figure 4. Theoretically derived frontier orbitals of (a) DFT optimized S_0 state and (b) TD-DFT optimized S_1 state for organoboron-based biphenyls (red: positive; green: negative; surface isovalue: 0.015), calculated with B3LYP function (basis sets: 6-31G(d) for H, B, C; and 6-31G+(d) for N). Hydrogen atoms are omitted for clarity.

DOI: 10.1021/acs.joc.5b02038
J. Org. Chem. 2015, 80, 10914−10924

Theoretical Calculations. To have a clear understanding of the underlying reasons for the observed experimental results, theoretical calculations were carried out using Gaussian 09 program.[27] Through theoretical calculation, we are going to clarify the effect of molecular structure on (1) absorption, in terms of longest absorption maxima and absorption intensity, and (2) fluorescence, in terms of longest maxima and fluorescence efficiency.

The optimized structures of S_0 state using density functional theory (DFT) show features that are reasonably consistent with those of X-ray structures (Table 3). Similarly, the boryl and amino groups are located at the same side of biphenyl axis in ***o,o′*-NMe$_2$**, but on two opposite sides in ***o,o′*-NBn$_2$**. In addition, the tricoordinate boron centers are planar, while geometries of nitrogen center are quite different. The geometry of nitrogen changes in a similar trend as observed for the X-ray crystal structures. Moreover, DFT calculations reproduced the short centroid−centroid distances between P1 and P4 in ***o,o′*-NMe$_2$** and ***o,p′*-NMe$_2$**, allowing intramolecular $\pi-\pi$ interactions between them.

Figures 4 and 5 show the pictorial drawings and energy levels of HOMOs and LUMOs, respectively. For all the organoboron-based biphenyls, their LUMOs are localized primarily on the dimesitylboryl phenyl moiety. Consequently, their LUMO energy levels (0.63−0.69 eV) are not very different (Figure 6).

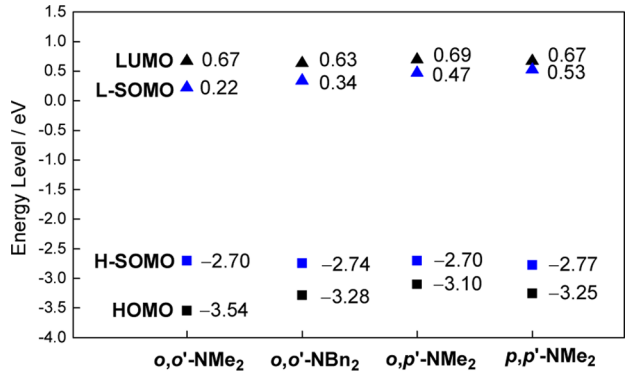

Figure 5. Theoretical energy levels of frontier orbitals for organoboron-based biphenyls, calculated with B3LYP function (basis sets: 6-31G(d) for H, B, C; and 6-31G+(d) for N).

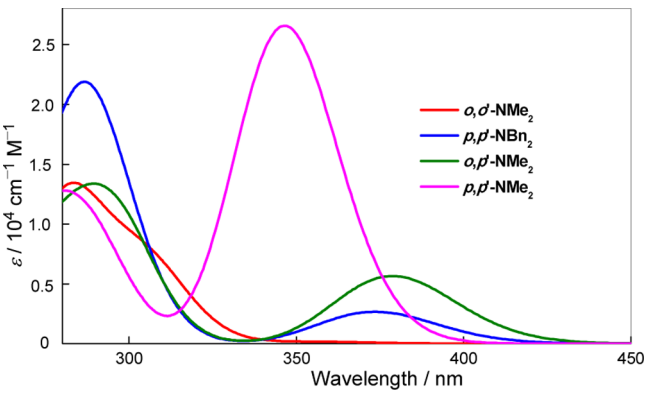

Figure 6. Theoretical UV−vis absorption spectra of organoboron-based biphenyls, calculated using TD-DFT with B3LYP function and "nstates = 10" (basis sets: 6-31G(d) for H, B, C; and 6-31G+(d) for N).

In contrast, great differences are observed in electron distribution and energy level of HOMOs. The HOMO of ***p,p′*-NMe$_2$** can spread over the whole biphenyl skeleton including NMe_2 substituent. However, the contribution of P2 to HOMO is much less efficient for other compounds, possibly due to their twisted structure and thus less efficient conjugation of biphenyl framework. Notably, the benzene ring P4 contributes to the HOMO to some extent for ***o,p′*-NMe$_2$** and ***o,o′*-NMe$_2$**, confirming the intramolecular $\pi-\pi$ interaction between P1 and P4. With regard to the HOMO energy level, ***o,p′*-NMe$_2$** shows highest HOMO energy level, and the HOMO energy level of ***o,o′*-NMe$_2$** is the most low-lying among the three regioisomeric organoboron-based biphenyls. In addition to the highly twisted structure of biphenyl skeleton, the significantly pyramidalized geometry of nitrogen center is probably another factor that accounts for the low-lying of HOMO energy level of ***o,o′*-NMe$_2$**. As the result of variation in HOMO energy level, the HOMO−LUMO gap first exhibits a decrease and then increase from ***p,p′*-NMe$_2$** to ***o,p′*-NMe$_2$** and **NMe$_2$**. From ***o,o′*-NMe$_2$** to ***o,o′*-NBn$_2$**, with the conformation change of biphenyl, the HOMO is greatly elevated, and thus HOMO−LUMO gap turns much narrower, although the electron-donating abilities of NBn_2 and NMe_2 are not very different. The elevation of HOMO is probably due to higher planarity of N center and biphenyl skeleton in ***o,o′*-NBn$_2$**, which would cause more efficient electron delocalization

In addition, to assign the absorptions of these organoboron-based biphenyls, time-dependent DFT (TD-DFT) calculations were conducted, and the related data are summarized in Table 4. The first excited state for all these all these molecules is assignable to the intramolecular CT transition from the HOMO to the LUMO. The transition energy of the first excited state changes in a similar trend as HOMO−LUMO energy gap. It is notable that their oscillator strengths of S_1 are quite different. The oscillator strength exhibits a substantial decrease from ***p,p′*-NMe$_2$** to ***o,p′*-NMe$_2$** and further ***o,o′*-NMe$_2$** (f = 0.0023 for ***o,o′*-NMe$_2$**; 0.078 for ***o,p′*-NMe$_2$**; 0.3667 for ***p,p′*-NMe$_2$**).[25a,b] With the change of biphenyl conformation, the oscillator strength increases from ***o,o′*-NMe$_2$** to ***o,o′*-NBn$_2$** (f = 0.0368 for ***o,o′*-NBn$_2$**). Especially, the oscillator strength of S_1 transition for ***o,o′*-NMe$_2$** is particularly low. Figure 6 shows the theoretically calculated UV−vis absorption spectra using TD-DFT, which are reasonably consistent with experiment UV−vis absorption spectra, in terms of spectra shape and intensity of longest absorption band.

To further shed a light on the difference in the intensity of longest band, the degree of HOMO−LUMO overlap was evaluated. According to quantum mechanics, a remarkable spatial overlap of orbitals involved in the light absorption process is necessary for a large transition dipole moment, which would lead to intense light absorption and high absorption extinction coefficient (ε). For all these organoboron-based biphenyls, the S_1 state is mainly dominated by the HOMO → LUMO transition. As a consequence, the evaluation on the HOMO−LUMO overlap will provide useful hints for the transition dipole moments and ε values. The HOMO−LUMO overlap can be quantified by an index Λ.[28] A larger Λ corresponds to more efficient HOMO−LUMO overlap. Indeed, ***o,o′*-NMe$_2$** has the smallest Λ, while Λ of ***p,p′*-NMe$_2$** is largest among three regioisomeric organoboron-based biphenyls (Λ = 0.0637 for ***o,o′*-NMe$_2$**; 0.103 for ***o,p′*-NMe$_2$**; 0.204 for ***p,p′*-NMe$_2$**). The Λ becomes larger from ***o,o′*-NMe$_2$** to ***o,o′*-NBn$_2$** (Λ = 0.0898 for ***o,o′*-NBn$_2$**). The difference in the

DOI: 10.1021/acs.joc.5b02038
J. Org. Chem. 2015, 80, 10914−10924

Table 4. Theoretical Photophysical Data of Organoboron-Based Biphenyls, Calculated Using TD-DFT with B3LYP Function[a]

	absorption				emission			
	dominant components (%)	E (eV)	λ (nm)	f	dominant components (%)	E (eV)	λ (nm)	f
***o,o′*-NMe$_2$**	HOMO→LUMO (98)	3.49	355	0.0023	H-SOMO→L-SOMO (100)	2.21	561	0.0012
***o,o′*-NBn$_2$**	HOMO→LUMO (99)	3.32	373	0.0368	H-SOMO→L-SOMO (99)	2.51	494	0.0266
***o,p′*-NMe$_2$**	HOMO→LUMO (99)	3.28	378	0.078	H-SOMO→L-SOMO (99)	2.61	475	0.0305
***p,p′*-NMe$_2$**	HOMO→LUMO (99)	3.58	346	0.3667	H-SOMO→L-SOMO (99)	2.95	421	0.2213

[a]Basis sets: 6-31G(d) for H, B, C; and 6-31G+(d) for N.

degree of HOMO−LUMO overlap probably can be rationalized by coplanarity of biphenyl framework. The higher coplanarity of biphenyl framework would lead to more efficient HOMO−LUMO overlap.

To clarify the effect of molecular structure on fluorescence properties, the first singlet excited-state structures (S_1) were also optimized using TD-DFT calculations. Relative to the ground state, the following structural features are notable for the optimized structure in S_1 state (Table 3). (1) The relative positions of boryl and amino groups remain unchanged for ***o,o′*-NMe$_2$** and ***o,o′*-NBn$_2$**, in which boryl and amino groups are still arranged at the same side and on opposite sides of biphenyl axis, respectively. (2) The NC_3 plane turns almost perfectly planar with the N1−C30 bond becoming shorter except for ***p,p′*-NMe$_2$**. In addition, these changes are most significant for ***o,o′*-NMe$_2$**, which shows most pyramidalized NC_3 geometry in the ground state. (3) Except for ***p,p′*-NMe$_2$**, the dihedral angle between P2 and BC_3 plane is reduced along with shortening of related B1−C19 bond, suggesting more efficient conjugation between vacant p orbital and P2 ring. Notably, the dihedral angle between P2 and BC_3 is smallest for ***o,o′*-NMe$_2$**, which also shows shortest B−C19 bond length. (4) In ***o,o′*-NMe$_2$**, ***o,o′*-NBn$_2$**, the torsion angle between P1 and P4 decreases, along with the shortening of P1−P4 centroid distance, suggesting stronger $\pi-\pi$ interaction between P1 and P4 in S_1 state.

It seems the electron distribution of frontier orbitals in S_1 state is not very different from that in S_0 state (Figure 4). In view of frontier orbital levels (Figure 5), the highest singly occupied orbital (H-SOMO) and lowest singly occupied orbital (L-SOMO) are elevated and lowered, respectively, from ***p,p′*-NMe$_2$** to ***o,p′*-NMe$_2$**, which might arise from effective $\pi-\pi$ interaction between P1 and P4 in S_1 state of ***o,p′*-NMe$_2$**. Notably, the difference of orbital energy level is mainly reflected in the L-SOMO for other three compounds, in contrast to the significant difference of LUMO in S_0 state. Interestingly, the L-SOMO of ***o,o′*-NMe$_2$** is most low-lying, which might be due to the efficient electron delocalization through vacant p orbital of boron center. Consistent with the change of energy level of frontier orbitals, TD-DFT calculated emission wavelength is longest for ***o,o′*-NMe$_2$** and shortest ***p,p′*-NMe$_2$** for the three regioisomeric organoboron-based biphenyls. And TD-DFT calculated emission is blue-shifted from ***o,o′*-NMe$_2$** to ***o,o′*-NBn$_2$** with the change of relative position of boryl and amino groups. The change trend of calculated fluorescence wavelength also correlates well with that of experimental results in cyclohexane (Table 4). Moreover, the smaller oscillator strength of ***o,o′*-NMe$_2$** than other compounds agrees well with the experimental trend in k_r values. The very low oscillator strength ***o,o′*-NMe$_2$** is presumably related to its poor spatial overlap between H-SOMO and L-SOMO.

All the organoboron-based biphenyls are characteristic of intramolecular CT transition, and thus they would have a more polar structure in the excited state than in the ground state. The dipole moments at the optimized S_0 and S_1 geometries and at the Franck−Condon geometries for emission and absorption are also calculated and are collected in Table 5. All these compounds have a very low dipole moment in the ground state but a very high dipole moment in the excited state. The least significant dipole change from ground state to the excited state is found for ***o,o′*-NMe$_2$**, while ***p,p′*-NMe$_2$** displays largest dipole moment change, which in good agreement with the change trend in the degree of HOMO−LUMO overlap.

Table 5. Theoretical Dipole Moments (debye) of Organoboron-Based Biphenyls, Calculated Using TD-DFT with B3LYP Function[a]

	S_0	S_1^{FC}	S_1	S_0^{FC}	S_1-S_0
***o,o′*-NMe$_2$**	1.56	13.92	12.90	1.64	11.34
***o,o′*-NBn$_2$**	1.08	16.25	16.41	1.42	15.33
***o,p′*-NMe$_2$**	2.26	17.11	18.63	2.40	16.37
***p,p′*-NMe$_2$**	2.52	28.48	30.06	2.79	27.54

[a]Calculated at the following points on the ground and lowest singlet excited-state surfaces: S_0, the optimized geometry of the ground state; S_1, the optimized geometry of the first singlet excited state; S_1^{FC}, the S_1 state at the FC geometry following excitation; and S_0^{FC}, the S_0 state at the FC geometry following emission. Basis sets: 6-31G(d) for H, B, C; and 6-31G+(d) for N

Although the accuracy of the calculated frontier energy levels, absorption, and emission energy is not sufficiently high by this level of calculation, these calculated results clearly support that the substitution position of boryl and amino groups as well as conformation of *o,o′*-substituted biphenyls have great influence on photophysical properties. The unique structure of ***o,o′*-NMe$_2$**, in which electron-donating NMe_2 and electron-accepting $BMes_2$ groups at *o,o′*-positions are located at same side of biphenyl axis with close B···N distance and direct B···N electronic interaction, is helpful achieve long emission wavelength and thus particularly large Stokes shift.

Fluorescence Solvatochromism. To verify the theoretical results about the polarity change from ground state to the excited state, the solvent effects on the absorption and emission spectra were also investigated, and the related data are summarized in Table 6. The three regioisomeric biphenyls ***o,o′*-NMe$_2$**, ***o,p′*-NMe$_2$**, and ***p,p′*-NMe$_2$** display remarkable solvatochromism on fluorescence while no obvious solvent dependence on absorption.[25a,b] Similarly, the fluorescence spectra of ***o,o′*-NBn$_2$** are also red-shifted with increased solvent polarity, while absorption spectra remain almost unchanged. These facts clearly denote that their structures are more polar in the excited state than in the ground state. To compare the degree of polarization in the excited state for these compounds, we employed the Lippert−Mataga equation (eq 1), in which C is a constant, μ_e and μ_g are the dipole moments in the exited state and ground state, respectively, $\Delta\nu$ is the Stokes shift,and

DOI: 10.1021/acs.joc.5b02038
J. Org. Chem. 2015, 80, 10914−10924

Table 6. UV−vis Absorption and Fluorescence Data of Organoboron-Based Biphenyls in Various Solvents

	solvent	λ_{abs} (nm)[a]	λ_{abs} (nm)	$\Delta\nu$ (cm^{-1})[b]	a[d]	$\Delta\mu$[e]
o,o′-NMe_2	cyclohexane	306	521	13485	7.53	14.8
	$CHCl_3$	307	547	14292		
	THF	307	551	14424		
	MeCN	303	580	15762		
o,o′-NBn_2	cyclohexane	362[c]	450	5402	8.32	17.7
	$CHCl_3$	364[c]	478	6552		
	THF	367[c]	492	6923		
	MeCN	385[c]	508	6289		
o,p′-NMe_2	cyclohexane	388	477	4809	7.73	19.4
	$CHCl_3$	385	520	6743		
	THF	395	541	6832		
	MeCN	386	570	8363		
p,p′-NMe_2	cyclohexane	369	409	2650	7.96	24.8
	$CHCl_3$	371	459	5168		
	THF	375	488	6175		
	MeCN	375	528	7727		

[a]Only the longest absorption maximum wavelengths are given. [b]Stokes shift. [c]Observed as a shoulder. [d]Radius of cavity calculated by using the optimized structure. [e]Calculated change in dipole moment ($\mu_e - \mu_g$) from the ground state to the excited state.

Δf is the solvent polarity and is given by eq 2, in which ε is the dielectric constant and n is the optical refractive constant. The Lippert−Mataga equation:

$$\Delta\nu = \nu_A - \nu_F = \frac{2\Delta f}{hca^3}(\mu_e - \mu_g)^2 + C \quad (1)$$

$$\Delta f = \frac{\varepsilon - 1}{2\varepsilon + 1} - \frac{n^2 - 1}{2n^2 + 1} \quad (2)$$

accounts for the general solvent effect and does not account for specific solvent−fluorophore interactions, for example, through hydrogen bonding. We indeed obtained linear relationships for the plots of $\Delta\nu$ as a function of Δf for these three compounds, as shown in Figure 7. From the slope of these plots, the change in the dipole moment ($\mu_e - \mu_g$) of the fluorophore upon electronic excitation was calculated assuming the molecular radius as the cavity radius.[29] The molecules under consideration are nonspherical in nature. The molecular radii were estimated from DFT calculations based on their DFT optimized structures using X-ray crystal structure as initial structure and listed in Table 6. The dipole moments changes were calculated and are also summarized in Table 5. The dipole moment changes between ground state and excited state are very large for all these biphenyls, confirming their emission come from the highly polarized excited state induced by intramolecular CT transition. In addition, the changes of dipole moment are very different with the change in substitution position of boryl and amino groups and steric effect of amino substituent. Among three regioisomeric biphenyls, *o,o′*-NMe_2 displays least dipole moment change from the ground state to the excited state. And the dipole moment change increase gradually from *o,o′*-NMe_2 to *o,p′*-NMe_2 and *o,p′*-NMe_2.[25a,b] Interestingly, *o,o′*-NBn_2 shows a larger dipole moment change than *o,o′*-NMe_2. The experimental results obviously agree well the theoretical calculation results.

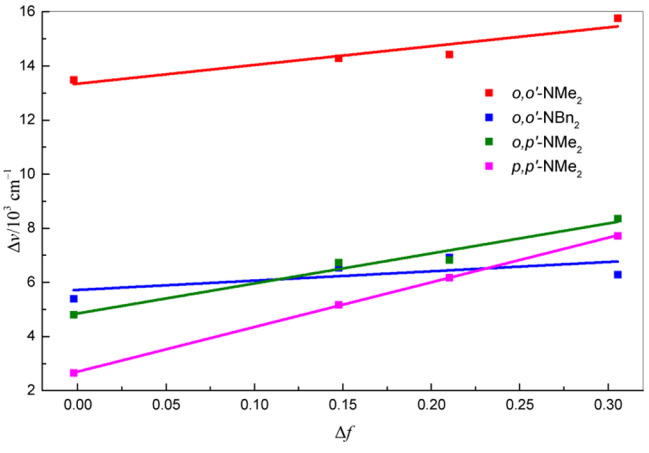

Figure 7. Lippert−Mataga plots of organoboron-based biphenyls.

Photophysical Properties in the Solid State. One fascinating property of *o,o′*-NMe_2 is its intense fluorescence in the solid state. So we next investigated the photophysical properties of these four organoboron-based biphenyls in the solid state. Their absorption and emission spectra in spin-coated film state are shown in Figure 8, and the related data are summarized in Table 7.

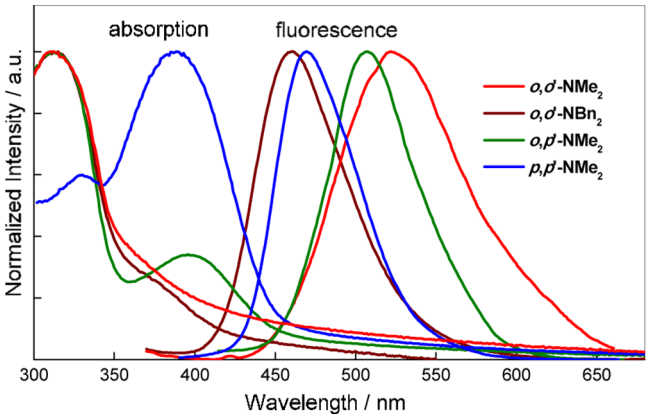

Figure 8. Absorption and fluorescence spectra of organoboron-based biphenyls in spin-coated films.

In view of the fluorescence spectra, it was found that the fluoresce spectra of *o,o′*-NMe_2 retains almost unchanged from nonpolar cyclohexane solution to spin-coated film. In contrast, other compounds display red shift in fluorescence to some extent, which is most prominent for *p,p′*-NMe_2 (red shift of

Table 7. UV−vis Absorption and Fluorescence Data for Biphenyls in Spin-Coated Films

	λ_{abs}[a] (nm)	λ_{em} (nm)	Φ_F[c]	$\Delta\nu$ (cm^{-1})	$\Delta\lambda$ (nm)	τ (ns)
o,o′-NMe_2	308	523	0.86	13347	215	34.5/58.3 (27/73)[d]
o,o′-NBn_2	373[b]	461	0.35	5117	88	13.1
o,p′-NMe_2	396	507	0.66	5528	111	16.5/19.6 (40/60)[d]
p,p′-NMe_2	389	470	0.65	4430	81	3.8/9.7 (72/28)[d]

[a]Only the longest absorption maximum wavelengths are shown. [b]Observed as a shoulder peak. [c]Absolute quantum yields determined by a calibrated integrating sphere system. [d]Amplitudes of the lifetimes given in parentheses.

DOI: 10.1021/acs.joc.5b02038
J. Org. Chem. 2015, 80, 10914−10924

emission from cyclohexane to spin-coated film: 11 nm for ***o,o′*-NBn$_2$**; 30 nm for ***o,p′*-NMe$_2$**, and 61 nm for ***p,p′*-NMe$_2$**). Even so, the emission wavelength of ***o,o′*-NMe$_2$** is still longest among these four compounds. It was interesting to notice that the quantum yield of ***o,o′*-NMe$_2$** is nearly doubled, while other compounds exhibit some decrease in quantum yield from cyclohexane solution to spin-coated film. As a consequence, the spin-coated film quantum yield of ***o,o′*-NMe$_2$** is highest among these biphenyls despite its relatively low quantum yield in cyclohexane solution. The time-resolved fluorescence measurements revealed that the three regioisomeric ***o,o′*-NMe$_2$**, ***o,p′*-NMe$_2$**, and ***p,p′*-NMe$_2$** show biexponential decays in the solid state and gave two components, which are longer than the corresponding lifetime in cyclohexane, especially for ***o,o′*-NMe$_2$** (Table 7). Thus, with the introduction of more substituents at the lateral position, the longer-lived excited state becomes more dominant. The characterization of these two components remains unclear at this moment.

CONCLUSION

In summary, we have comprehensively investigated a series of organoboron-based biphenyls, in which electron-donating amino group and electron-accepting boryl groups are introduced at different positions or the substituents of amino group are different for *o,o′*-substituted biphenyls. Their single-crystal X-ray structures, photophysical properties, in solution and solid state, and theoretical calculations were fully characterized. It was found that the conformation of biphenyl is tunable via choosing amino group with different steric effect for *o,o′*-substituted compounds. When NMe$_2$ is introduced, ***o,o′*-NMe$_2$** displays a conformation, in which NMe$_2$ and BMes$_2$ are located at same side of biphenyl axis with a close distance and thus direct electronic attraction between boron and nitrogen centers. However, when NBn$_2$ with large steric effect is introduced in ***o,o′*-NBn$_2$**, the amino and boryl groups are arranged on two opposite sides of biphenyls axis. In addition, the photophysical properties are highly dependent on not only the substitution position of boryl and amino groups but also the conformation of biphenyl skeleton for *o,o′*-substituted compounds. Considering intense fluorescence of these compounds in both solution and solid state, the tuning of emission wavelength becomes possible through control of substitution position and conformation, which would provide alternative methods for the property tuning in addition to the traditional ways through attaching chemical substituents with various electronic effect to π core unit of different conjugation extension. Moreover, ***o,o′*-NMe$_2$** exhibits the longest emission wavelength but the shortest absorption wavelength, and thus largest Stokes shift among these four organoboron-based biphenyls. The theoretical calculations demonstrated that the unique structure of ***o,o′*-NMe$_2$**, in which boryl and amino located at the same side of biphenyl axis with close B···N distance and direct B···N electronic interaction, is helpful to stabilize L-SOMO in the exited state. The above results are expected to provide some important clues for not only property tuning of organoboron-based molecules but also for the design of fascinating emissive materials with high solid-state fluorescence efficiency and large Stokes shift. Further research along this line is underway in our group.

EXPERIMENTAL SECTION

General. Proton nuclear magnetic resonance (^{1}H NMR) spectra were recorded at 300 MHz in $CDCl_3$ and carbon nuclear magnetic resonance (^{13}C NMR) were measured at 75 MHz/100 MHz in $CDCl_3$. Mass spectra (MS) were obtained using an electrospray ionization time-of-flight (ESI-TOF) mass spectrometer. The spin-coated films were prepared by spinning the dichloromethane solutions (3 mg mL^{-1}) onto quartz plates at 1000 rpm for 30 s. The solid-state quantum yields were measured from the freshly spin-coated film using a calibrated integrating sphere system. 2-Amino-2′-bromobiphenyl[30] and dimesitylboron fluoride[31] were prepared according to the reported literature. All reactions were carried out under nitrogen atmosphere.

Computational Methods. All calculations were conducted by using the Gaussian 09 program.[27] The functional of B3LYP was used for all the calculations.[32] The employed atomic basis sets were 6-31G(d) for H, B, C and 6-31G+(d) for N atoms, respectively. The ground-state geometries were optimized starting from X-ray crystallographic structure. To ensure that the optimized geometry was at a minimum, all geometry optimizations were followed by a frequency calculation, and only positive frequencies were obtained. Based on the optimized ground-state structure, the vertical transitions were calculated by TD-DFT method. The TD-DFT geometry optimizations of the S_1 state starting from X-ray crystallographic structure and optimized structure of S_0 state produced very similar geometry. The discussions are mainly based on the results using X-ray crystallographic structure as initial geometry. In addition, frequency calculations were performed at the S_1 optimized geometries to confirm local minima had been found.

*2-Bromo-2′-(N,N-dibenzylamino)biphenyl (**1**).* To a mixture of 2-amino-2′-bromobiphenyl (3.0 g, 12 mmol) and K_2CO_3 (6.6 g, 48 mmol) in CH_3CN (90 mL) was added BnBr (4.9 g, 28.8 mmol) under a stream of nitrogen. The mixture was heated at reflux at 90 °C for 2 days. After the mixture was cooled to room temperature, a saturated solution of NaCl was added, and the aqueous layer was extracted with CH_2Cl_2. The combined organic layer was dried over anhydrous Na_2SO_4, filtered, and concentrated under reduced pressure. The resulting mixture was subjected to a silica gel column chromatography (20/1 petroleum ether/ethyl acetate, R_f = 0.25) to afford 4.4 g (10.3 mmol) of **1** in 86% yield as white solids: Mp 80.0−81.5 °C; ^{1}H NMR ($CDCl_3$, 300 MHz): δ = 7.70 (d, J = 7.8 Hz, 1H), 7.42 (t, J = 7.5 Hz, 1H), 7.30−7.21 (m, 10H), 7.15−6.99 (m, 6H), 3.96 ppm (s, 4H); ^{13}C NMR ($CDCl_3$, 100 MHz):[33] δ = 149.3, 142.0, 138.0, 136.4, 133.2, 132.5, 132.1, 129.2, 128.6, 128.5, 128.1, 127.0, 124.1, 122.7, 122.5, 55.9 ppm; HRMS (ESI-TOF): m/z calcd for $C_{26}H_{23}BrN$: 428.1014 [M + H]$^+$; found 428.1007.

*2-Dimesitylboryl-2′-(N,N-dibenzylamino)biphenyl (**o,o′-NBn$_2$**).* To a solution of **1** (428 mg, 1 mmol) in anhydrous THF (20 mL) was added a hexane solution of *n*-BuLi (0.75 mL, 1.6 M, 1.2 mmol) dropwise by syringe at −78 °C under a stream of nitrogen. The mixture was stirred at the same temperature for 1 h. A solution of dimesitylboron fluoride (534 mg, 2.0 mmol) in anhydrous THF (5 mL) was added to the reaction mixture via syringe. The reaction mixture was warmed to room temperature and stirred overnight. The reaction was quenched with saturated solution of NaCl, and the aqueous layer was extracted with CH_2Cl_2. The combined organic layer was dried over anhydrous Na_2SO_4, filtered, and concentrated under reduced pressure. The resulting mixture was subjected to a silica gel column chromatography (50/1 petroleum ether/CH_2Cl_2, R_f = 0.30) to afford 120 mg (0.2 mmol) of ***o,o′*-NBn$_2$** in 20% yield as pale cyan solids: Mp 164.0−165.0 °C; ^{1}H NMR ($CDCl_3$, 300 MHz): δ = 8.06 (br, 1H), 7.50−7.41 (m, 2H), 7.32−7.29 (m, 2H), 7.24−7.22 (m, 6H), 7.03−6.86 (m, 6H), 6.76 (d, J = 7.8 Hz, 1H), 6.53 (br, 4H), 3.90 (s, 4H), 2.16 (s, 6H), 1.94 (s, 12H) ; ^{13}C NMR ($CDCl_3$, 100 MHz): δ = 148.6, 145.0, 143.1, 141.0, 138.7, 137.5, 136.3, 135.8, 134.8, 131.6, 129.7, 128.8, 128.0, 127.2, 127.1, 126.6, 122.5, 121.8, 56.2, 23.8, 21.3 ppm; HRMS (ESI-TOF): m/z calcd for $C_{44}H_{45}BN$: 598.3645 [M + H]$^+$; found: 598.3642.

*4-Bromo-4′-(N,N-dibenzylamino)biphenyl (**2**).* To a mixture of [4-(dibenzylamino)phenyl]boronic acid (632 mg, 2.0 mmol), 4-iodobromobenzene (622 mg, 2.4 mmol), K_2CO_3 (2.21 g, 16.0 mmol), $Pd(OAc)_2$ (22 mg, 0.10 mmol) and PPh_3 (80 mg, 0.30 mmol) were added degassed toluene (40 mL) and H_2O/EtOH (3/1, 8 mL) under a stream of nitrogen. The reaction mixture was heated at reflux

DOI: 10.1021/acs.joc.5b02038
J. Org. Chem. 2015, 80, 10914−10924

overnight. The mixture was cooled to room temperature, and then extracted with CH_2Cl_2. The combined organic layer was dried over anhydrous Na_2SO_4, filtered, and concentrated under reduced pressure. The residue was purified by silica gel column chromatography (10:1 petroleum ether/CH_2Cl_2, R_f = 0.30) to afford (603 mg, 1.4 mmol) of **2** in 70% yield as a white solids: Mp 123.0−124.5 °C; ^{1}H NMR ($CDCl_3$, 300 MHz): δ = 7.48 (d, J = 8.7 Hz, 2H), 7.39−7.31 (m, 8H), 7.27−7.24 (m, 6H), 6.80 (d, J = 8.7 Hz, 2H), 4.69 ppm (s, 4H); ^{13}C NMR ($CDCl_3$, 75 MHz): δ = 148.8, 140.0, 138.3, 131.7, 128.7, 128.1, 127.72, 127.67, 127.0, 126.6, 120.0, 112.7, 54.3 ppm; HRMS (ESI-TOF): m/z calcd for $C_{26}H_{23}BrN$: 428.1014 $[M + H]^+$; found: 428.1015.

*4-Dimesitylboryl-2′-(N,N-dibenzylamino)biphenyl (**p,p′-NBn$_2$**).* This compound was prepared essentially in the same manner for ***o,o′*-NBn$_2$** using **2** (257 mg, 0.6 mmol), anhydrous THF (30 mL), *n*-BuLi (0.45 mL, 1.6 M, 0.72 mmol), and dimesitylboron fluoride (312 mg, 2.0 mmol) in anhydrous THF (8 mL). The purification by a silica gel column chromatography (petroleum ether, R_f = 0.28) afforded 140 mg (0.234 mmol) of ***p,p′*-NBn$_2$** in 39% yield as pale yellow solids: Mp 207.5−208.5 °C; ^{1}H NMR ($CDCl_3$, 300 MHz): δ = 7.52−7.49 (m, 6H), 7.36−7.26 (m, 10H), 6.82−6.79 (m, 6H), 4.70 (s, 4H), 2.30 (s, 6H), 2.03 ppm (s, 12H); ^{13}C NMR ($CDCl_3$, 75 MHz): δ = 148.8, 144.2, 141.9, 140.8, 138.4, 138.2, 137.3, 128.7, 128.1, 128.0, 127.1, 126.7, 125.3, 112.9, 54.4, 23.5, 21.2 ppm; HRMS (ESI-TOF): m/z calcd for $C_{44}H_{45}BN$: 598.3645 $[M + H]^+$; found: 598.3645.

*X-ray Crystal Structure Analysis of **o,o′-NBn$_2$**.*[34] Single crystals of ***o,o′*-NBn$_2$** for X-ray crystal analysis were obtained by recrystallization from a MeOH/CH_2Cl_2 mixed solvent. Intensity data were collected at 293 K with Mo Kα radiation (λ = 0.710 Å) and graphite monochromator. A total of 8853 reflections were measured at a maximum 2θ angle of 50.0°, of which 6126 were independent reflections (R_{int} = 0.0538). The structure was solved by direct methods (SHELEXL-97)[35] and refined by the full-matrix least-squares on F^2 (SHELEXL-97).[35] All non-hydrogen atoms were refined anisotropically, and all hydrogen atoms except for those of the disordered solvent molecules were placed using AFIX instructions. The crystal data are as follows: $C_{44}H_{44}BN$; F_W = 597.61; crystal size 0.20 × 0.20 × 0.20 mm^3, triclinic, *P*-1, a = 8.512(2) Å, b = 12.728(4) Å, c = 17.319(5) Å, V = 1750.1(9) Å^3, Z = 2, D_c = 1.134 g cm^{-3}. The refinement converged to R_1 = 0.0640, wR_2 = 0.1903 ($I > 2\sigma(I)$), GOF = 0.905.

■ ASSOCIATED CONTENT

Supporting Information

These materials is available free of charge via the Internet at The Supporting Information is available free of charge on the ACS Publications website at DOI: 10.1021/acs.joc.5b02038.

Thermal ellipsoid plot of the X-ray structure of ***o,o′*-NBn$_2$**, Cartesian coordinates of DFT optimized structures in ground state (S_0) and TD-DFT optimized structures in the first excited state (S_1). ^{1}H NMR and ^{13}C NMR spectra of all new compounds, HSQC spectrum of **1** (PDF)

Crystallographic data (CIF)

■ AUTHOR INFORMATION

Corresponding Author

*E-mail: chzhao@sdu.edu.cn.

Notes

The authors declare no competing financial interest.

■ ACKNOWLEDGMENTS

This work was supported by the National Nature Science Foundation of China (21272141, 21572120) and Promotive Research Fund For Excellent Young and Middle-aged Scientists of Shandong Province (BS 2012CL021n).

■ REFERENCES

(1) (a) Neto, B. A. D.; Carvalho, P. H. P. R.; Correa, J. R. *Acc. Chem. Res.* **2015**, *48*, 1560−1569. (b) Saeed, M. A.; Le, H. T. M.; Miljanić, Q. Š. *Acc. Chem. Res.* **2014**, *47*, 2074−2083. (c) Ding, D.; Liu, B.; Tang, B. Z. *Acc. Chem. Res.* **2013**, *46*, 2441−2453. (d) Grimsdale, A. C.; Chan, K. L.; Martin, R. E.; Jokisz, P. G.; Holmes, A. B. *Chem. Rev.* **2009**, *109*, 897−1091. (e) Müllen, K.; Scherf, U. *Organic Light-Emitting Devices*; Wiley-VCH: Weinheim, 2006.

(2) Lakowicz, J. R. *Principles of Fluorescence Spectroscopy*; Springer: New York, 2006.

(3) (a) Hong, Y.; Lam, J. W. Y.; Tang, B. Z. *Chem. Soc. Rev.* **2011**, *40*, 5361−5388. (b) Shimizu, M.; Hiyama, T. *Chem. - Asian J.* **2010**, *5*, 1516−1531. (c) Babu, S. S.; Kartha, K. K.; Ajayaghosh, A. *J. Phys. Chem. Lett.* **2010**, *1*, 3413−3424. (d) Anthony, S. P. *ChemPlusChem* **2012**, *77*, 518−531.

(4) (a) Grell, M.; Bradley, D. D. C.; Ungar, G.; Hill, J.; Whitehead, K. S. *Macromolecules* **1999**, *32*, 5810−5817. (b) Lemmer, U.; Heun, S.; Mahrt, R. F.; Scherf, U.; Hopeier, M.; Siegner, U.; Göbel, E. O.; Müllen, K.; Bässeler, H. *Chem. Phys. Lett.* **1995**, *240*, 373−378.

(5) (a) Qin, T.; Zhou, G.; Scheiber, H.; Bauser, R. E.; Baumgarten, M.; Anson, C. E.; List, E. J. W.; Müllen, K. *Angew. Chem., Int. Ed.* **2008**, *47*, 8292−8296. (b) Langhals, H.; Krotz, O.; Polborn, K.; Mayer, P. *Angew. Chem., Int. Ed.* **2005**, *44*, 2427−2428. (c) Ozdemir, T.; Atilgan, S.; Kutuk, I.; Yildirim, L. T.; Tulek, A.; Bayindir, M.; Akkaya, E. U. *Org. Lett.* **2009**, *11*, 2105−2107. (d) Lu, H.; Wang, Q.; Gai, L.; Li, Z.; Deng, Y.; Xiao, X.; Lai, G.; Shen, Z. *Chem. - Eur. J.* **2012**, *18*, 7852−7861. (e) Fu, G.-L.; Pan, H.; Zhao, Y.-H.; Zhao, C.-H. *Org. Biomol. Chem.* **2011**, *9*, 8141−8146.

(6) (a) Xie, Z.; Yang, B.; Li, F.; Cheng, G.; Liu, L.; Yang, G.; Xu, H.; Ye, L.; Hanif, M.; Liu, S.; Ma, D.; Ma, Y. *J. Am. Chem. Soc.* **2005**, *127*, 14152−14153. (b) He, F.; Xu, H.; Yang, B.; Duan, Y.; Tian, L.; Huang, K.; Ma, Y.; Liu, S.; Feng, S.; Shen, J. *Adv. Mater.* **2005**, *17*, 2710−2714.

(7) (a) Hong, Y.; Lam, J. W. Y.; Tang, B. Z. *Chem. Soc. Rev.* **2011**, *40*, 5361−5388. (b) Qin, A.; Tang, B. Z. *Aggregation-induced Emission: Fundamentals, Applications*; Wiley-VCH: New York, 2013.

(8) (a) Zhang, Z.; Xu, B.; Su, J.; Shen, L.; Xie, Y.; Tian, H. *Angew. Chem., Int. Ed.* **2011**, *50*, 11654−11657. (b) Wang, B.; Wang, Y.; Hua, J.; Jiang, Y.; Huang, J.; Qian, S.; Tian, H. *Chem. - Eur. J.* **2011**, *17*, 2647−2655. (c) Ning, Z.; Chen, Z.; Zhang, Q.; Yan, Y.; Qian, S.; Cao, Y.; Tian, H. *Adv. Funct. Mater.* **2007**, *17*, 3799−3807.

(9) (a) Kim, S.; Zhang, A.; He, G. S.; Bharali, D. J.; Pudavar, H. E.; Baev, A.; Prasad, P. N. *Adv. Funct. Mater.* **2006**, *16*, 2317−2323. (b) An, B. K.; Kwon, S. K.; Jung, S. D.; Park, S. Y. *J. Am. Chem. Soc.* **2002**, *124*, 14410−14415. (c) Gu, X.; Yao, J.; Zhang, G.; Zhang, C.; Yan, Y.; Zhao, Y.; Zhang, D. *Chem. - Asian J.* **2013**, *8*, 2362−2369.

(10) (a) Würthner, F.; Kaiser, T. E.; Saha-Möller, C. R. *Angew. Chem., Int. Ed.* **2011**, *50*, 3376−3410. (b) Kaiser, T. E.; Wang, H.; Stepanenko, V.; Würthner, F. *Angew. Chem., Int. Ed.* **2007**, *46*, 5541−5544.

(11) (a) Saragi, T. P. I.; Spehr, T.; Siebert, A.; Fuhrmann-Lieker, T.; Salbeck, J. *Chem. Rev.* **2007**, *107*, 1011−1065. (b) Poriel, C.; Cocherel, N.; Rault-Berthelot, J.; Vignau, L.; Jeannin, O. *Chem. - Eur. J.* **2011**, *17*, 12631−12645. (c) Thirion, D.; Rault-Berthelot, J.; Vignau, L.; Poriel, C. *Org. Lett.* **2011**, *13*, 4418−4421. (d) Wang, J.; Wan, W.; Jiang, H.; Gao, Y.; jiang, X.; Lin, H.; Zhao, W.; Hao, J. *Org. Lett.* **2010**, *12*, 3874−3877. (e) Poriel, C.; Rault-Bertjelot, J.; Thirion, D.; Barrière, F.; Vignau, L. *Chem. - Eur. J.* **2011**, *17*, 14031−14046.

(12) (a) Zhao, C.-H.; Wakamiya, A.; Inukai, Y.; Yamaguchi, S. *J. Am. Chem. Soc.* **2006**, *128*, 15934−15935. (b) Wakamiya, A.; Mori, K.; Yamaguchi, S. *Angew. Chem., Int. Ed.* **2007**, *46*, 4273−4276. (c) Zhao, C.-H.; Wakamiya, A.; Yamaguchi, S. *Macromolecules* **2007**, *40*, 3898−3900. (d) Zhao, C.-H.; Sakuda, E.; Wakamiya, A.; Yamaguchi, S. *Chem. - Eur. J.* **2009**, *15*, 10603−10612.

(13) (a) Zhao, C.-H.; Zhao, Y.-H.; Pan, H.; Fu, G.-L. *Chem. Commun.* **2011**, *47*, 5518−5520. (b) Fu, G.-L.; Zhang, H.-Y.; Yan, Y.-Q.; Zhao, C.-H. *J. Org. Chem.* **2012**, *77*, 1983−1990.

(14) (a) Shimizu, M.; Takeda, Y.; Higashi, M.; Hiyama, T. *Angew. Chem., Int. Ed.* **2009**, *48*, 3653−3656. (b) Shimizu, M.; Kaki, R.;

DOI: 10.1021/acs.joc.5b02038
J. Org. Chem. 2015, 80, 10914−10924

Takeda, Y.; Hiyama, T.; Nagai, N.; Yamagishi, H.; Furutani, H. *Angew. Chem., Int. Ed.* **2012**, *51*, 4095−4099.
(15) For reviews of boron-based π-electron materials: (a) Wade, C. R.; Broomsgrove, A. E. J.; Aldridge, S.; Gabbaï, F. P. *Chem. Rev.* **2010**, *110*, 3958−3984. (b) Jäkle, F. *Chem. Rev.* **2010**, *110*, 3985−4022. (c) Hudson, Z. M.; Wang, S. *Acc. Chem. Res.* **2009**, *42*, 1584−1596 and references cited herein..
(16) (a) Entwistle, C. D.; Collings, J. C.; Steffen, A.; Pålsson, L.-O.; Beeby, A.; Albesa-Jové, D.; Burke, J. M.; Batsanov, A. S.; Howard, J. A. K.; Mosely, J. A.; Poon, S.-Y.; Wong, W.-Y.; Ibersiene, F.; Fathallah, S.; Boucekkine, A.; Halet, J.-F.; Marder, T. B. *J. Mater. Chem.* **2009**, *19*, 7532−7544. (b) Zhou, G.; Ho, C.-L.; Wong, W.-Y.; Wang, Q.; Ma, D.; Wang, L.; Lin, Z.; Marder, T. B.; Beeby, A. *Adv. Funct. Mater.* **2008**, *18*, 499−511. (c) Weber, L.; Eickhoff, D.; Marder, T. B.; Fox, M. A.; Low, P. J.; Dwyer, A. D.; Tozer, D. J.; Schwedler, S.; Brockhinke, A.; Stammler, H.-G.; Neumann, B. *Chem. - Eur. J.* **2012**, *18*, 1369−1382 and references cited herein..
(17) (a) Lequan, M.; Lequan; Ching, K. C.; Barzoukas, M.; Fort, A.; Lahoucine, H.; Bravic, G.; Chasseau, D.; Gaultier, J. *J. Mater. Chem.* **1992**, *2*, 719−725. (b) Lequan, M.; Lequan, R. M.; Chane-Ching, K.; Callier, A.-C.; Barzoukas, M.; Fort, A. *Adv. Mater. Opt. Electron.* **1992**, *1*, 243−247. (c) Lequan, M.; Lequan, R. M.; Ching, K. C. *J. Mater. Chem.* **1991**, *1*, 997−999. (d) Branger, C.; Lequan, M.; Lequan, R. M.; Barzoukas, M.; Fort, A. *J. Mater. Chem.* **1996**, *6*, 555−558.
(18) (a) Jia, W.-L.; Bai, D.-R.; McCormick, T.; Liu, Q.-D.; Motala, M.; Wang, R.-Y.; Seward, C.; Tao, Y.; Wang, S. *Chem. - Eur. J.* **2004**, *10*, 994−1006. (b) Jia, W.-L.; Feng, X.-D.; Bai, D.-R.; Lu, Z.-H.; Wang, S.; Vamvounis, G. *Chem. Mater.* **2005**, *17*, 164−170. (c) Jia, W.-L.; Moran, M. J.; Yuan, Y.-Y.; Lu, Z.-H.; Wang, S. *J. Mater. Chem.* **2005**, *15*, 3326−3333.
(19) (a) Noda, T.; Shirota, Y. *J. Am. Chem. Soc.* **1998**, *120*, 9714−9715. (b) Noda, T.; Ogawa, H.; Shirota, Y. *Adv. Mater.* **1999**, *11*, 283−285. (c) Noda, T.; Shirota, Y. *J. Lumin.* **2000**, *87*−*89*, 1168−1170. (d) Shirota, Y.; Kinoshita, M.; Noda, T.; Okumoto, K.; Ohara, T. *J. Am. Chem. Soc.* **2000**, *122*, 11021−11022. (e) Kinoshita, M.; Fujii, N.; Tsuzuki, T.; Shirota, Y. *Synth. Met.* **2001**, *121*, 1571−1572. (f) Doi, H.; Kinoshita, M.; Okumoto, K.; Shirota, Y. *Chem. Mater.* **2003**, *15*, 1080−1089.
(20) (a) Lin, S.-L.; Chan, L.-H.; Lee, R.-H.; Yen, M.-Y.; Kuo, W.-J.; Chen, C.-T.; Jeng, R.-J. *Adv. Mater.* **2008**, *20*, 3947−3952. (b) Chen, L.; Jiang, Y.; Nie, H.; Lu, P.; Sung, H. H. Y.; Williams, I. D.; Kwok, H. S.; Huang, F.; Qin, A.; Zhao, Z.; Tang, B. *Adv. Funct. Mater.* **2014**, *24*, 3621−3630. (c) Yuan, W. Z.; Chen, S.; Lam, J. W. Y.; Deng, C.; Lu, P.; Sung, H.-H.-Y.; Williams, I. D.; Kwok, H. S.; Zhang, Y.; Tang, B. Z. *Chem. Commun.* **2011**, *47*, 11216−11218.
(21) (a) Yamaguchi, S.; Akiyama, S.; Tamao, K. *J. Am. Chem. Soc.* **2001**, *123*, 11372−11375. (b) Yamaguchi, S.; Shirasaka, T.; Akiyama, S.; Tamao, K. *J. Am. Chem. Soc.* **2002**, *124*, 8816−8817. (c) Kubo, Y.; Yamamoto, M.; Ikeda, M.; Takeuchi, M.; Shinkai, S.; Yamaguchi, S.; Tamao, K. *Angew. Chem., Int. Ed.* **2003**, *42*, 2036−2040.
(22) (a) Solé, S.; Gabbaï, F. P. *Chem. Commun.* **2004**, 1284−1285. (b) Melaimi, M.; Gabbaï, F. P. *J. Am. Chem. Soc.* **2005**, *127*, 9680−9681. (c) Chiu, C.-W.; Gabbaï, F. P. *J. Am. Chem. Soc.* **2006**, *128*, 14248−14249. (d) Lee, M. H.; Agou, T.; Kobayashi, J.; Kawashima, T.; Gabbaï, F. P. *Chem. Commun.* **2007**, 1133−1135. (e) Hudnall, T. W.; Melaïmi, M.; Gabbaï, F. P. *Org. Lett.* **2006**, *8*, 2747−2749.
(23) (a) Sundararaman, A.; Victor, M.; Varughese, R.; Jäkle, F. *J. Am. Chem. Soc.* **2005**, *127*, 13748−13749. (b) Parab, K.; Venkatasubbaiah, K.; Jäkle, F. *J. Am. Chem. Soc.* **2006**, *128*, 12879−12885. (c) Li, H.; Sundararaman, A.; Venkatasubbaiah, K.; Jäkle, F. *J. Am. Chem. Soc.* **2007**, *129*, 5792−5793.
(24) (a) Zhao, Y.-H.; Pan, H.; Fu, G.-L.; Lin, J.-M.; Zhao, C.-H. *Tetrahedron Lett.* **2011**, *52*, 3832−3835. (b) Xu, Q.-W.; Wang, C.; Sun, Z.-B.; Zhao, C.-H. *Org. Biomol. Chem.* **2015**, *13*, 3032−3039.
(25) (a) Pan, H.; Fu, G.-L.; Zhao, Y.-H.; Zhao, C.-H. *Org. Lett.* **2011**, *13*, 4830−4833. (b) Yan, Y.-Q.; Li, Y.-B.; Wang, J.-W.; Zhao, C.-H. *Chem. - Asian J.* **2013**, *8*, 3164−3176. (c) Wang, C.; Jia, J.; Zhang, W.-N.; Zhang, H.-Y.; Zhao, C.-H. *Chem. - Eur. J.* **2014**, *20*, 16590−16601.
(26) Brouwer, A. M. *Pure Appl. Chem.* **2011**, *41*, 2073−2075.
(27) Frisch, M. J.; Trucks, G. W.; Schlegel, H. B.; Scuseria, G. E.; Robb, M. A.; Cheeseman, J. R.; Scalmani, G.; Barone, V.; Mennucci, B.; Petersson, G. A.; Nakatsuji, H.; Caricato, M.; Li, X.; Hratchian, H. P.; Izmaylov, A. F.; Bloino, J.; Zheng, G.; Sonnenberg, J. L.; Hada, M.; Ehara, M.; Toyota, K.; Fukuda, R.; Hasegawa, J.; Ishida, M.; Nakajima, T.; Honda, Y.; Kitao, O.; Nakai, H.; Vreven, T.; Montgomery, J. A., Jr.; Peralta, J. E.; Ogliaro, F.; Bearpark, M.; Heyd, J. J.; Brothers, E.; Kudin, K. N.; Staroverov, V. N.; Kobayashi, R.; Normand, J.; Raghavachari, K.; Rendell, A.; Burant, J. C.; Iyengar, S. S.; Tomasi, J.; Cossi, M.; Rega, N.; Millam, J. M.; Klene, Knox, M. J. E.; Cross, J. B.; Bakken, V.; Adamo, C.; Jaramillo, J.; Gomperts, R.; Stratmann, R. E.; Yazyev, O.; Austin, A. J.; Cammi, R.; Pomelli, C.; Ochterski, J. W.; Martin, R. L.; Morokuma, K.; Zakrzewski, V. G.; Voth, G. A.; Salvador, P.; Dannenberg, J. J.; Dapprich, S.; Daniels, A. D.; Farkas, O.; Foresman, J. B.; Ortiz, J. V.; Cioslowski, J.; Fox, D. J. *Gaussian 09*, Revision A.02, Gaussian, Inc.: Wallingford, CT, 2009.
(28) Peach, M. J. G.; Benfield, P.; Helgaker, T.; Tozer, D. J. *J. Chem. Phys.* **2008**, *128*, 044118−1−044118−8.
(29) Zhang, L.; Clark, R. J.; Zhu, L. *Chem. - Eur. J.* **2008**, *14*, 2894−2903.
(30) Pan, X.; Wilcox, C. S. *J. Org. Chem.* **2010**, *75*, 6445−6451.
(31) Eisch, J. J.; Shafii, B.; Odom, J. D.; Rheingold, A. L. *J. Am. Chem. Soc.* **1990**, *112*, 1847−1853.
(32) (a) Stephens, P. J.; Delin, F. J.; Chabalowski, C. F.; Frisch, M. J. *J. Phys. Chem.* **1994**, *98*, 11623−11627. (b) Becke, A. D. *J. Chem. Phys.* **1993**, *98*, 5648−5652. (c) Lee, C.; Yang, W.; Parr, R. G. *Phys. Rev. B: Condens. Matter Mater. Phys.* **1988**, *37*, 785−789. (d) Liu, X.; Xu, Z.; Cole, J. M. *J. Phys. Chem. C* **2013**, *117*, 16584−16595.
(33) In ^{13}C NMR of **1**, there is only one 15 aromatic carbon signal, one less than the theoretical number. According to the HSQC spectrum of **1**, two carbon nuclei are accidentally isochronous at the chemical shift of 127.0 ppm.
(34) Crystal data for ***o*,*o*′-NBn$_2$**: see the Supporting Information. CCDC 1051899 contains lementary crystallographic data for this paper. These data can be obtained free of charge from The Cambridge Crysallographic Data Centre via www.ccdc.cam.ac.uk/data_request/cif.
(35) Sheldrick, G. M. *SHELX-97, Program for the Refinement of Crystal Structure*; University of Göttingen: Götingen, Germany, 1997.

DOI: 10.1021/acs.joc.5b02038
J. Org. Chem. 2015, 80, 10914−10924